# Computation of Transonic Flow About Helicopter Rotor Blades

Rimon Arieli* and Michael E. Tauber†
*NASA Ames Research Center, Moffett Field, California*
David A. Saunders‡
*Informatics General Corporation, Palo Alto, California*
and
David A. Caughey§
*Cornell University, Ithaca, New York*

**An inviscid, nonconservative, three-dimensional full-potential flow code, ROT22, has been developed for computing the quasi-steady flow about a lifting rotor blade. The code is valid throughout the subsonic and transonic regime. Calculations from the code are compared with detailed laser velocimeter measurements made in the tip region of a nonlifting rotor at a tip Mach number of 0.95 and zero advance ratio. In addition, comparisons are made with chordwise surface pressure measurements obtained in a wind tunnel for a nonlifting rotor blade at transonic tip speeds at advance ratios from 0.40 to 0.50. The overall agreement between theoretical calculations and experiment is very good. A typical run on a CRAY X-MP computer requires about 30 CPU seconds for one rotor position at transonic tip speed.**

## Nomenclature

| | |
|---|---|
| $a$ | = speed of sound |
| $c$ | = blade chord |
| $C_p$ | = pressure coefficient, see Eq. (8) |
| $C_p^*$ | = pressure coefficient at sonic speed |
| $M$ | = Mach number |
| $M_s$ | = Mach number of approaching airstream at blade station $r_s$, see Eq. (9) |
| $p$ | = static pressure |
| $q_1, q_2, q_3$ | = velocity components in $x,y,z$ directions, respectively |
| $r_s$ | = spanwise (radial) blade station from center of rotation |
| $R$ | = blade radius from center of rotation to tip |
| $\bar{R}$ | = $r_s/R$ |
| $t$ | = time |
| $\bar{U}, \bar{V}$ | = chordwise and normal velocity components divided by $\Omega R$, respectively |
| $V$ | = forward flight velocity of vehicle |
| $\bar{W}$ | = spanwise (radial) velocity component divided by $\Omega R$ |
| $x,y$ | = chordwise and normal coordinates, respectively |
| $z$ | = spanwise (radial) coordinate |
| $\alpha$ | = angle of attack |
| $\gamma$ | = ratio of specific heats |
| $\mu$ | = advance ratio, see Eq. (7) |
| $\Phi$ | = full velocity potential function |
| $\phi$ | = perturbation velocity potential function |
| $\psi$ | = azimuth angle of blade, measured counterclockwise from tail |
| $\Omega$ | = angular velocity of rotor |

Received April 8, 1985; revision received Sept. 9, 1985. 

*Senior Fellow, National Research Council. Member AIAA.
†Research Scientist. Associate Fellow AIAA.
‡Task Manager.
§Professor. Associate Fellow AIAA.

## Introduction

THE development of computer codes to analyze the three-dimensional (3-D) flowfield about rotor blades has been hindered by the mathematical complexity associated with modeling the physical behavior. When a helicopter is in forward flight, a rotor blade is exposed to widely different flowfields, depending on its azimuthal position in the rotor disk. The blade that is "advancing" into the oncoming airstream experiences high dynamic pressures and needs only small angles of attack to produce adequate lift to maintain lateral trim. On the opposite side of the disk, the "retreating" blade experiences low dynamic pressure and must operate at high angles of attack to develop the same amount of lift as the advancing blade. Analysis of the retreating blade flow is complicated by dynamic stall phenomena that are induced by the high angle of attack and that dominate the flow. In contrast to the unsteady viscous flow effects on the retreating blade, the advancing blade in high-speed forward flight experiences small angles of attack, and the transonic flowfield near the tip is amenable to inviscid flow analysis.

Several investigators have previously developed analytical models for transonic rotor flows. The first three-dimensional, transonic calculations for flow over rotor blades were performed by Caradonna and Isom,[1] using small-disturbance theory. The calculations were made for a nonlifting rotor in hover such that the tip speed was representative of forward flight. Subsequently, this steady-state formulation was extended to the unsteady, forward flight case[2]; however, the spanwise freestream velocity component due to changing blade position was assumed to be small and was incompletely modeled. Grant[3] included all freestream velocity components in his solution of the transonic small-disturbance equation for nonlifting forward flight, but assumed quasi-steady flow.

In contrast to the situation for rotary wing aircraft, computer codes for solving the three-dimensional flowfield about fixed lifting wings have been available for some years. One of the more widely used is a full potential code, FL022, developed by Jameson and Caughey.[4] Results from it are

compared with experimental data in Ref. 5. The FL022 code provides an inviscid solution to the full-potential equation using exact surface tangency boundary conditions; the formulation is nonconservative with respect to mass flux. A successive line overrelaxation solution procedure is used.

The FL022 code was extended to calculate the inviscid flowfield about a lifting rotor blade in forward flight and is referred to as code ROT22. The detailed description of ROT22 is given in Ref. 6; only the main features are outlined here. The location of the blade axis of rotation is arbitrary. Although the flowfield varies with the blade azimuthal angle, it is computed in a quasi-steady manner. However, the treatment of the rotational terms in the equations assures that both the spanwise and cross-flow terms are correctly modeled. Because the full-potential equation and the exact tangency boundary condition are used rather than the small-disturbance approximations, subsonic and transonic flow over airfoils of finite thickness and bluntness can be realistically modeled. There are no inherent geometric limitations; airfoil section and chord can be varied, as well as angle of attack, collective pitch, twist, and flapping angle.

In the remainder of the paper, a brief description of the salient features of the analysis is presented. This is followed by a comparison of calculations from the code with experimental measurements made in hover at a transonic tip speed and at conditions simulating very high-speed forward flight.

## Brief Description of Analysis

As noted previously, complete mathematical modeling of the flowfield about a rotor is a very complex task and is beyond the state-of-the-art. Simplifying assumptions are required to make the problem tractable over the even part of the rotor disk. Beyond the assumptions inherent in the full-potential equation, the simplifications embodied in the model are: 1) a single-blade analysis, 2) an approximate wake-induced inflow, 3) a special mathematical treatment of the vortex sheet behind the blade, and 4) a quasi-steady flowfield.

The complete potential flow—including the centrifugal and Coriolis terms due to rotation about the vertical, or $y$, axis—can be rewritten in a blade-attached coordinate system as:¶

$$(a^2-q_1^2)\Phi_{xx}+(a^2-q_2^2)\Phi_{yy}+(a^2-q_3^2)\Phi_{zz}-2q_1q_2\Phi_{xy}-2q_1q_3\Phi_{xz}-2q_2q_3\Phi_{yz}+\Omega^2(x\Phi_x+z\Phi_z)=\Phi_{tt}+2q_1\Phi_{xt}+2q_2\Phi_{yt}+2q_3\Phi_{zt} \quad (1)$$

Here $q_1$, $q_2$, and $q_3$ are the velocity components in the $x$, $y$, and $z$ directions, respectively, defined by

$$q_1=\Phi_x+\Omega z, \qquad q_2=\Phi_y, \qquad q_3=\Phi_z-\Omega x$$

where $\Phi$ is the full velocity potential and $\Omega$ is the rotation rate (in rad/unit time).

The local speed of sound $a$ is related to the velocity potential by the Bernoulli equation

$$a^2=a_\infty^2+((\gamma-1)/2)V^2-((\gamma-1)/2)[2\Phi_t+\Phi_x^2+\Phi_y^2+\Phi_z^2+2\Omega(z\Phi_x-x\Phi_z)] \quad (2)$$

where $V$ is the forward flight speed and $\psi$ the blade azimuth angle. The time and spatial derivatives of the full velocity potential are related to the derivatives of the perturbation potential $\phi$ by

$$\Phi_t=\Omega V\cos\alpha(x\cos\psi-z\sin\psi)+\phi_t$$

$$\Phi_x=V\cos\alpha\sin\psi+\phi_x$$

$$\Phi_y=V\sin\alpha+\phi_y$$

$$\Phi_z=V\cos\alpha\cos\psi+\phi_z \quad (3)$$

where $\alpha$ is the angle of attack of the rotor disk.

If the flow is assumed to be quasi-steady, all the time derivatives of the perturbation potential in the above equations vanish, and the resulting equations can be written as

$$(a^2-q_1^2)\phi_{xx}+(a^2-q_2^2)\phi_{yy}+(a^2-q_3^2)\phi_{zz}-2q_1q_2\phi_{xy}-2q_1q_3\phi_{xz}-2q_2q_3\phi_{yz}+\Omega^2(x\phi_x+z\phi_z)-2\Omega V\cos\alpha(\phi_x\cos\psi-\phi_z\sin\psi)=0 \quad (4)$$

$$a^2=a_\infty^2-((\gamma-1)/2)[\phi_x^2+\phi_y^2+\phi_z^2+2\Omega(z\phi_x-x\phi_z)+2V\cos\alpha(\phi_x\sin\psi+\phi_z\cos\psi)+2V\phi_y\sin\alpha] \quad (5)$$

It should be noted that the effects of rotation are still included with the quasi-steady assumption. Although the time history is removed from the solution for forward flight, Eqs. (4) and (5) and the boundary conditions retain a timelike dependence by being a function of rotor position. The far-field boundary conditions are

$$(\Phi_x)_\infty=V\sin\psi\cos\alpha, \quad (\Phi_y)_\infty=V\sin\alpha, \quad (\Phi_z)_\infty=V\cos\psi\cos\alpha \quad (6)$$

For the near field, the exact surface tangency boundary condition is used so that all velocities are evaluated at the blade surface.

In the solution of the potential equation (4), several transformations are made to map the flow into a region tailored for efficient numerical computation (see Ref. 4). However, two regions of the flowfield are given special treatment in the analysis. The first is the trailing vortex sheet that is assumed to leave the blade at the bisector of the trailing-edge angle. The vertical location of the vortex sheet is not part of the solution; instead, the vortex sheet is assumed to lie in a (transformed) coordinate plane across which the normal velocity and pressure are continuous. This assumption introduces two limitations: first, the downstream extent of the vortex sheet is confined to one revolution or less; second, the rollup of the tip vortex cannot be described. In the horizontal plane, the vortex sheet (wake) follows an essentially kinematic path. The wake-induced rotor inflow from a preceding blade can be modeled by placing one or two line vortices in the flowfield. The strengths of the vortices are determined by the lift on the blade; however, the locations must be specified (implying some uncertainty). Recently, Egolf and Sparks[7] have improved the wake modeling by coupling a lifting-line far wake with ROT22. The modified code yields very good pressure comparisons with data for lifting blades into the transonic speed regime. The comparisons published so far were limited to hover.

The second region receiving special treatment was the tip region. The required mapping outboard of the tip produced a singularity from the tip toward the outer computational boundary. Where the singular line intersected each $x$-$y$ plane, the point singularity (only) was treated by locally solving the two-dimensional potential-flow equation as in FLO22.

¶The analysis can be performed in an inertial coordinate system. In this case, the potential equation is simple, but the boundary conditions are both geometrically complex and unsteady. Further, if the time-dependent terms are not retained, that is, if a quasi-steady assumption is invoked, then all the essential features of rotor flow, such as spanwise velocity gradients and centrifugal and Coriolis forces, are eliminated. For these reasons, blade-fixed coordinates were adopted as the most practical reference system.

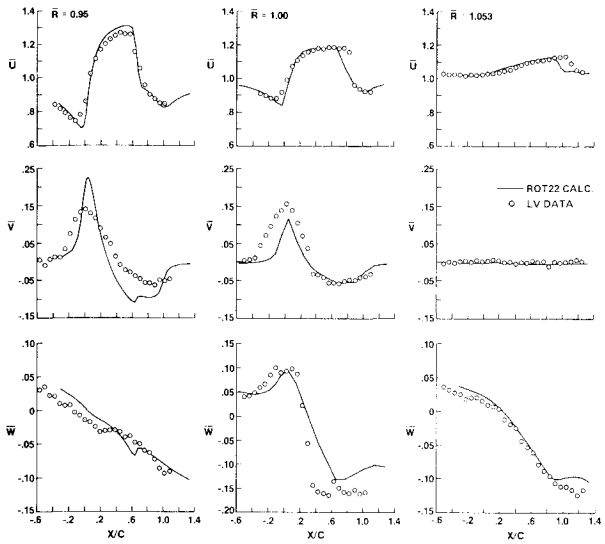


**Fig. 1 ROT22 and laser velocimetry measurement comparison in hover for $M_{tip} = 0.95$, $y/c = 0.0838$.**

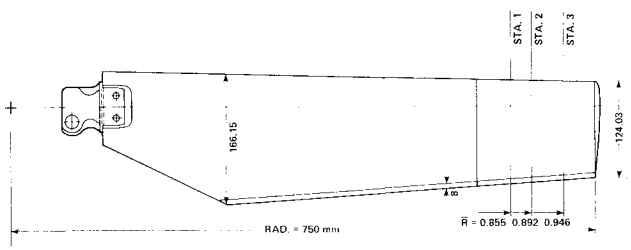


**a) Straight blade.**

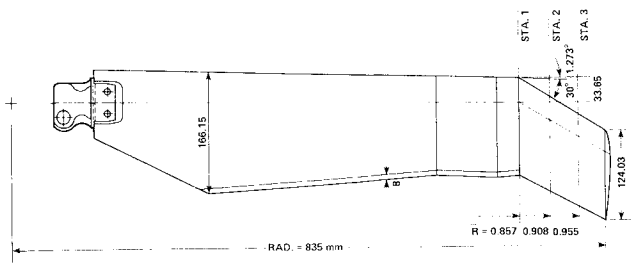


**b) Swept-tip blade.**

**Fig. 2 ONERA blade geometries.**

Before presenting results obtained with this computational model, it is worthwhile to discuss some of the consequences of the assumptions made in developing the code. The omission of viscous effects limits the effective applicability of the model to advancing blades where the viscous effects are not dominant (as they are for retreating blade flows). However, computations of retreating blade tip flows can be made to study the inviscid pressure gradients, etc. Atlhough flow over lifting blades can be calculated, the present wake-induced inflow model introduces some uncertainty, as previously discussed. Most of the better quality data are for nonlifting rotors; nonetheless, significant insight into rotor flows and the predictive ability of the code can be gained through comparison with these cases. The use of the potential-flow equation to model a rotor flow results in a significant simplification over using the Euler equations because much less computer time and memory are required to solve one potential equation than to solve the four conservation equations.

The effect of assuming a quasi-steady flow was first studied by Isom[8] using the small-disturbance theory. Isom studied the effect of advance ratio

$$\mu = \frac{V}{\Omega R}\cos\alpha \tag{7}$$

on the time dependence of the flowfield and concluded that the quasi-steady approximation was valid for small advance ratios; however, no numerical limits were given. (An advance ratio of 0.3-0.4 is typical of modern helicopters in high-speed forward flight.) Assuming quasi-steady flow permits computing the flowfield about the blade at one azimuth angle. This speeds the computation by nearly two orders of magnitude in comparison with a fully unsteady calculation. In an unsteady computation, the azimuth angle can be advanced only a fraction of a degree between time steps as the blade advances one-half revolution or more.[9] The quasi-steady assumption will be assessed in the next section, where results from the code are compared with experimental measurements.

## Comparisons with Experimental Data

Computations made using ROT22 were compared with experimental measurements on model rotors at transonic tip speeds. The comparisons were made with measurements taken in the vicinity of the rotor tips, where the flow is inherently three-dimensional. The first experiment consisted of nonintrusive laser velocimeter (LV) measurements of the three orthogonal velocity components in the neighborhood of the tip of the rotor in hover. In the second test chosen for comparison, surface pressures were measured near the tip on both straight and swept-tip model rotors at high advance ratios around the entire rotor disk. Both experiments were performed on nonlifting blades; the data are among the best in the literature.

## Model Configurations and Test Conditions for Velocity Measurements

The test was performed[10,11] in a large chamber about 10 m per side, with special ducting designed to minimize room circulation. The rotor consisted of two cantilever-mounted, manually adjustable blades. The blades were untwisted and untapered with symmetric NACA 0012 airfoil sections and an aspect ratio of 12. The blade tips were cut off squarely, normal to the planform. The rotor radius and chord were 104.5 cm (41.16 in.) and 7.62 cm (3.0 in.), respectively.

The laser velocimetry measurement was made at zero advance ratio and a tip Mach number of 0.95. The experiment consisted of measuring the three orthogonal velocity components in the neighborhood of the blade tip over a chordwise distance of two chords and a radial distance of about one chord. The laser velocimeter was a two-component system and used the fringe mode forward scatter technique with the 4880 and 5145 Å lines of an argon-ion laser. The overall system was specifically designed to measure all three components of induced velocity of a hovering rotor by taking data at two different azimuthal positions 90 deg apart. With a spanwise view of the tip as it swept by, one spectral line measured the induced streamwise velocity component while the other measured the induced vertical velocity component. Translation of both transmitting and receiving optics along the test chamber walls provided a chordwise view of the approaching or retreating tip, thus permitting the radial and vertical induced velocities to be measured. The effective sensing volume was approximately 0.2 mm in diam and 3 mm long, with the axis aligned in the plane of the beams. To enhance data acquisition rate, aerosol seeding was used; the mean aerosol diameter was about 0.7 $\mu$m. Conditional sampling techniques were employed to "freeze" the flowfield as the rotor swept past the fixed probe volume. A once-per-revolution pulse was used to activate the laser velocimeter electronics each time the rotor approached the

probe focal volume. Signals were then recorded during rotor transit past the focal volume. Readings from an event synchronizer were used to calculate two instantaneous velocity components and time of arrival. From these determinations, ensemble averages were generated throughout the blade-passing period and velocities were calculated for each data window. The induced velocity components were measured in an inertial (room-fixed) coordinate system. (However, aerodynamic properties of moving bodies are normally calculated in body-fixed coordinates. Therefore, the measured velocity components were transformed into blade-fixed coordinates for comparison with the ROT22 values.)

### Computation of Velocities

The flowfield over the entire blade was calculated using ROT22 in its efficient, fully vectorized form on a CRAY X-MP, in about 30 s of CPU time. The code output consisted of the $\bar{U}$, $\bar{V}$, and $\bar{W}$ velocity components (nondimensionalized by the rotational tip speed), the pressure coefficients, and local Mach numbers. A computational grid of 120 cells chordwise, 16 vertically, and 32 spanwise was used. About two-thirds of the spanwise computational stations were on the blade; the remainder were in the field, inboard and outboard of the blade. Nonuniform spanwise grid spacing was used to enhance resolution in the tip region and, in addition, to place a computational plane at the 95% radial blade station, where one set of measurements was made. (Three spanwise grid planes were located on the outer 5% of the blade and five outboard of the tip.) The two remaining radial measurement stations located at the blade tip and 2.17 cm beyond the tip were matched by linearly interpolating the computed velocity values. (It was undesirable to place a computational plane at the blade tip since the velocity gradients are very steep at that location. The ROT22 code normally places the tip between computational span stations, but this spacing can be altered.) For the present computation/experiment comparison, special provisions were made for interpolating between computational mesh points for the velocity components along horizontal lines of constant $y$ and between vertical planes.

### Comparison with LV Data

The comparisons presented in Fig. 1 between the calculated and measured velocities were made at a tip Mach number of 0.95 and at a height above the centerline of the blade of 0.084 chord length. The three velocities shown, $\bar{U}$, $\bar{V}$, and $\bar{W}$, are the chordwise, vertical, and radial components, respectively; all have been nondimensionalized by the tip velocity. The three chordwise scans were made at radial stations located 0.686 chord length inboard of the tip, at the tip, and 0.727 chord length beyond the tip.

Before assessing the agreement between the measurements and calculations, it is worthwhile to note some of the shortcomings associated with each result. Since the LV scan inboard of the tip was made less than 2 mm above the maximum thickness line of the blade, light reflecting from the blade surface degraded the signal used to determine the $\bar{V}$ velocity component. Also, the steepness of the velocity gradients at the blade tip could affect the measurements and did affect the computation. Computationally, the chordwise velocity component was affected by interpolation in the radial direction, causing the shock to appear diffused. Therefore, the agreement with experiment is not quite as good at the blade tip as inboard or beyond the tip.

The chordwise velocity component $\bar{U}$ is typically an order of magnitude larger than the vertical component $\bar{V}$ and the cross-flow velocity $\bar{W}$. Since the magnitude of the pressures and loads are proportional to the square root of the sum of the squares of the velocities, the accurate prediction of the (large) $\bar{U}$ component is essential. Note that in Fig. 1 the peak $\bar{U}$ velocity is overpredicted by a maximum of only 4% at $\bar{R}=0.95$. The shock location is also closely predicted, although beyond the tip it is about 0.1 chord length too far forward. Substantially greater disagreement exists in the (smaller) vertical $\bar{V}$ velocity comparisons. Here the differences approach 30-40% of the peak values, although the trends are well predicted. However, inaccuracies exist in the data at $\bar{R}=0.95$, as well as in the calculation at the blade tip as previously mentioned. The cross-flow component $\bar{W}$, although small, is well predicted, despite some scatter in the data at the tip. In view of the complexity of the flowfield, the agreement with the measurements was considered very good.

Therefore, the code should be useful in the study of transonic blade noise, which is thought to be caused by the propagation of the shock forming on the blade into the far field.[12] In fact, the ability of the code to predict correctly the

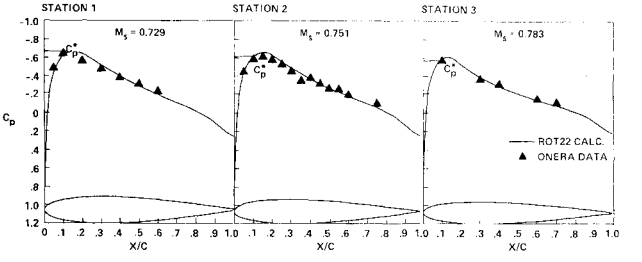


a) $\mu=0.4$, $\psi=60$ deg.

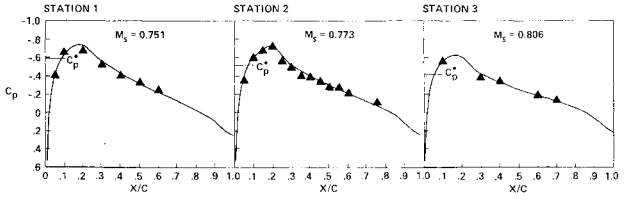


b) $\mu=0.4$, $\psi=90$ deg.

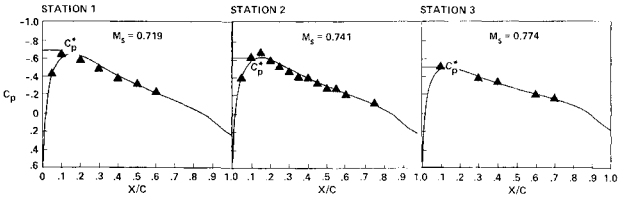


c) $\mu=0.4$, $\psi=120$ deg.

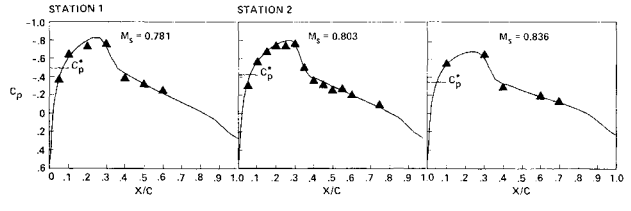


d) $\mu=0.45$, $\psi=90$ deg.

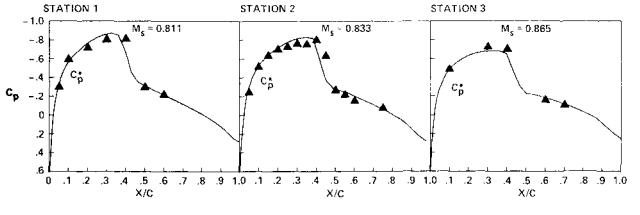


e) $\mu=0.5$, $\psi=90$ deg.

**Fig. 3 ROT22 and experimental pressure comparison for straight blade at spanwise locations indicated in Fig. 2a.**

shock strength, and nearly to predict the shock location beyond the tip, has been used to study rotor tip shapes that show promise of reducing transonic noise.[13] Thus, the good agreement between calculations and experiment enhances confidence in the ability of the ROT22 code to predict flowfields, pressures, and loads under the present conditions. Extension of the range of applicability of the code to high-speed forward flight is discussed next.

## Model Configurations and Test Conditions for Pressure Measurements

The pressure measurements used were made by ONERA[14,15] on modified Alouette helicopter tail rotor blades having nonlifting, symmetrical airfoil sections. The test was conducted with the rotor mounted on a stand in the wind tunnel; rotor speed and tunnel velocities were varied to achieve advance ratios ranging from 0.4 to 0.55. Two different rotor blade configurations were tested as illustrated in Fig. 2: one had a nearly straight leading edge and a 75-cm radius from the center of rotation; the second configuration (which had a radius of 83.5 cm) had 30 deg of leading-edge sweep on the outer 15%. Both blades had symmetric NACA four-digit airfoils, varying in thickness-to-chord ratio from 17% at the widest chord station to 9% at the tip.

Instrumentation on both blades consisted of three chordwise rows of dynamic pressure transducers, nominally at the 85%, 90%, and 95% radial stations. To achieve the desired instrumentation density, two tips were built for each configuration. The straight tips were nearly identical. However, because of fabrication difficulties, the swept tips differed somewhat, thus introducing some scatter in the data, especially at the middle, most densely instrumented station. Mean instantaneous pressures were computer-averaged; values were measured at 256 blade azimuthal positions. On the straight blade, the thickness-to-chord ratios at the instrumented stations were 13.1%, 12.15%, and 10.6%; while for the swept-tip blade the ratios were 13.5%, 12%, and 10.5%.

### Computation of Pressures

The flowfields over both blades were calculated for advance ratios of 0.4, 0.45, and 0.50. A computational grid of 120 cells chordwise, 16 vertically, and 24 spanwise was used for the straight blade; resolution was more critical for the swept-tip blade, and the number of spanwise stations was increased to 32. About two-thirds of the spanwise computational stations were on the blade; the remainder were in the field inboard and outboard of the blade. For the straight blade, the spanwise mesh spacing was adjusted so that a computational plane was located at the middle (0.892) instrumented station while, for the swept-tip blade, the crank in the tip (0.857 station) was matched. The pressure coefficients were linearly interpolated between the nearest computational stations for the other two radial stations. The pressure coefficient was defined as

$$C_p = \frac{1}{0.7M_s^2}\left(\frac{p}{p_\infty} - 1\right) \tag{8}$$

where the section Mach number was

$$M_s = (\Omega r_s + V\sin\psi)/a_\infty \tag{9}$$

Here $a_\infty$ is the freestream speed of sound, and the subscript $s$ refers to the blade radial station.

### Comparisons with Pressure Data

The calculated pressures in the tip regions of both blades were compared with measured values on the advancing blade. At an advance ratio of 0.4, comparisons were made from 60 to 120 deg. In addition, comparisons were also made at the important 90-deg azimuth angle at the very high advance ratios of 0.45 and 0.5 since this blade position is critical for predicting peak transonic noise[13] and drag.[14] Although advance ratios of 0.45 or higher exceed those of present helicopters, they might be encountered by future high-speed rotorcraft.

Theory and experiment compared well for the straight blade at an advance ratio of 0.4 at all three azimuth angles (see Figs. 3a-3c). At the 90-deg position (Fig. 3b), the tip Mach number was 0.84, resulting in a sizable region of supersonic flow. However, at 120 deg the flow was entirely subsonic. At the higher advance ratios of 0.45 and 0.5, the tip Mach numbers were 0.87 and 0.90, respectively. The agreement with the data at the 90-deg blade position was

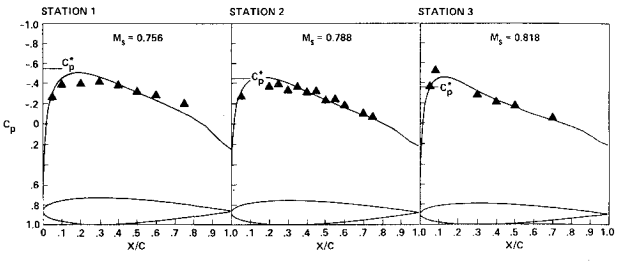


a) $\mu = 0.4$, $\psi = 60$ deg.

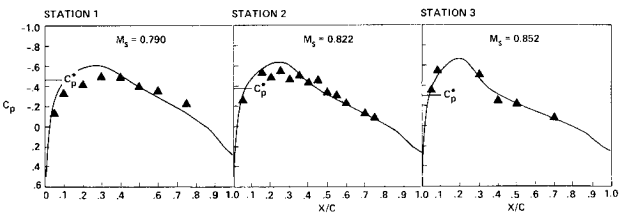


b) $\mu = 0.4$, $\psi = 90$ deg.

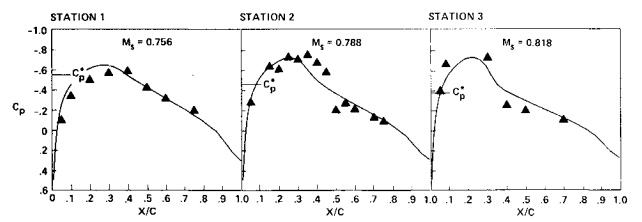


c) $\mu = 0.4$, $\psi = 120$ deg.

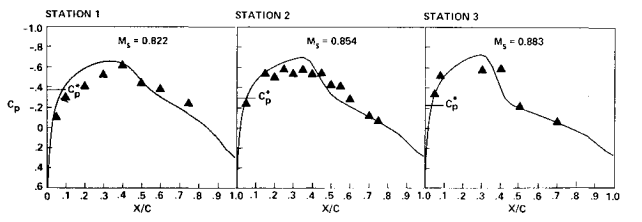


d) $\mu = 0.45$, $\psi = 90$ deg.

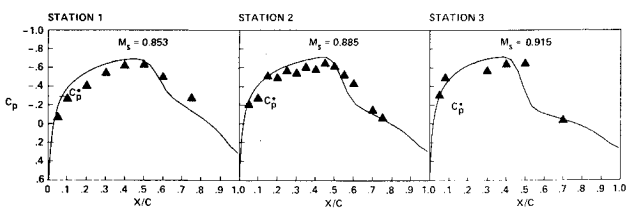


e) $\mu = 0.5$, $\psi = 90$ deg.

**Fig. 4 ROT22 and experimental pressure comparison for swept-tip blade at spanwise locations indicated in Fig. 2b.**

again good (see Figs. 3d and 3e). The swept-tip blade represents a more complex geometry than the straight, and experienced higher tip Mach numbers since the tip speed was increased from 200 to 210 m/s. At the advance ratio of 0.40, the maximum tip Mach number was 0.88. In general, the agreement (see Figs. 4a-4c) was not quite as good as it was for the straight blade. However, there was also more scatter in the data for the swept-tip cases possibly caused by inaccuracies in model construction. At the station where the crank in the planform occurs, the pressure expansion rate near the leading edge is somewhat overpredicted. It is possible that viscous effects were responsible, owing to the abrupt change in leading-edge sweep. At the higher advance ratios of 0.45 and 0.5, the tip Mach numbers reached 0.91 and 0.94, respectively, resulting in large regions of supersonic flow and strong shock waves (see Figs. 4d and 4e). The calculations again compared well with the data at the 90-deg blade azimuth angle. In view of the quasi-steady nature of the formulation, the ROT22 code gave remarkably good results at high advance ratios, especially at the critical 90-deg blade position.

## Concluding Remarks

The development of ROT22, the first three-dimensional computer code to solve the inviscid full-potential equation for the flow about a lifting helicopter rotor blade, has been described. The assumptions and approximations were discussed. The main simplifications were those of inviscid, quasi-steady, potential-flow simulation of the induced inflow, and treatment of the vortex sheet behind the blade. Calculations from the code were compared with measurements made in the inherently three-dimensional flow of the tip region and on the surface of nonlifting blades at transonic tip speeds. Calculated values of the three orthogonal velocity components agreed well with LV-measured velocities in the tip region of a blade rotating at a tip Mach number of 0.95 and with zero advance ratio. Further high-speed comparisons were made at advance ratios from 0.4 to 0.5, using surface pressures measured on straight and swept-tip blades. In view of the quasi-steady nature of the formulation, the code gave remarkably good results at the high advance ratios, especially at the important 90-deg blade azimuth position. The surface pressure comparisons supplement previous ones made over the entire rotor disk.[16] In Ref. 16 it was shown that when the flow on the blade was subsonic or moderately supersonic so that the terminating shocks were not too strong, the calculations agreed well with data. The unsteadiness of the flow affected only strong shock waves in the second quadrant, well beyond 90 deg, when the peak tip Mach number exceeded 0.9. Since the angle of incidence of the advancing blade in the vicinity of 90 deg is usually small (i.e., the lift coefficient is low), the code can be used with reasonable confidence to predict the important tip region flowfield, especially the occurrence, strength, and location of shock waves causing high drag and noise.

## References

[1]Caradonna, F. X. and Isom, M. P., "Subsonic and Transonic Potential Flow Over Helicopter Rotor Blades," *AIAA Journal*, Vol. 10, Dec. 1972, pp. 1606-1612.

[2]Caradonna, F. X. and Isom, M. P., "Numerical Calculation of Unsteady Transonic Potential Flow Over Helicopter Rotor Blades," *AIAA Journal*, Vol. 14, April 1976, pp. 482-488.

[3]Grant, J., "Calculation of the Supercritical Flow Over the Tip Region of Non-Lifting Rotor Blade at Arbitrary Azimuth," Royal Aircraft Establishment Tech. Rept. 77180, Dec. 1977.

[4]Jameson, A. and Caughey, D. A., "Numerical Calculation of the Transonic Flow Past a Swept Wing," Courant Institute of Mathematical Sciences, New York University, New York, C00-3077-140, June 1977.

[5]Henne, P. A. and Hicks, R. M., "Wing Analysis Using a Transonic Potential Flow Computation Method," NASA TM-78464, July 1978.

[6]Arieli, R. and Tauber, M. E., "Analysis of the Quasi-Steady Flow About an Isolated Lifting Helicopter Rotor Blade," Joint Institute for Aeronautics and Acoustics, Stanford University, Stanford, CA, TR-24, Aug. 1979.

[7]Egolf, T. A. and Sparks, S. P., "Hovering Rotor Airload Prediction Using a Full Potential Flow Analysis with Realistic Wake Geometry," presented at the 41st Annual Forum of the American Helicopter Society, Ft. Worth, TX, May 1985.

[8]Isom, M. P., "Unsteady Subsonic and Transonic Potential Flow over Helicopter Rotor Blades," NASA CR-2463, Oct. 1974.

[9]Chattot, J. J., "Calculation of Three-Dimensional Unsteady Transonic Flow Past Helicopter Blades," NASA TP-1721, Oct. 1980.

[10]Owen, F. K., Orngard, G. M., and McDevitt, T., "Laser Velocimeter Measurements of Model Helicopter Rotor Flow Fields," NASA CR177345, July 1984.

[11]Owen, F. K. and Tauber, M. E., "Measurement and Prediction of Model Rotor Flow Fields," AIAA Paper 85-1558, July 1985.

[12]Schmitz, F. H. and Yu, Y. H., "Transonic Rotor Noise —Theoretical and Experimental Comparison," Paper No. 22, 6th European Powered Lift Aircraft Forum, 1980.

[13]Tauber, M. E., "Computerized Aerodynamic Design of a Transonically 'Quiet' Blade," American Helicopter Society Paper A-84-40-46, May 1984.

[14]Caradonna, F. X. and Philippe, J. J., "The Flow over a Helicopter Blade Tip in the Transonic Regime," *Vertica*, Vol. 2, 1978, pp. 43-60.

[15]Monnerie, B. and Philippe, J. J., "Aerodynamic Problems of Helicopter Blade Tips," *Vertica*, Vol. 2, 1978, pp. 217-231.

[16]Tauber, M. E., Change, I. C., Caughey, D. A., and Philippe, J. J., "Comparison of Calculated and Measured Pressures on Straight and Swept-Tip Model Rotor Blades," NASA TM-85872, Dec. 1983.